Journal of Sustainability for Energy
https://www.acadlore.com/journals/JSE

Enhancing Energy Efficiency in Sow Houses: An Annual Temperature Regulation System Employing Heat Recovery and Photovoltaic-Thermal Technology

Yulu Liu, Kuo-Yi Lin*

Business College, Guilin University of Electronic Technology, 541214 Guangxi, China

* Correspondence: Kuo-Yi Lin (kylink1008@hotmail.com)

Received: 05-08-2023 **Revised:** 06-13-2023 **Accepted:** 06-21-2023

Citation: Y. L. Liu and K.-Y. Lin, "Enhancing energy efficiency in sow houses: An annual temperature regulation system employing heat recovery and photovoltaic-thermal technology," *J. Sustain. Energy*, vol. 2, no. 2, pp. 76–90, 2023. https://doi.org/10.56578/jse020204.

Abstract: This study proposes a novel annual temperature regulation system for sow houses, integrating heat recovery and photovoltaic-thermal (PV/T) technology to optimize energy utilization efficiency and economic benefits. Mathematical models of key system components are developed and validated using published data, yielding a maximum error of 14.48%. A numerical simulation assesses the system's operating characteristics across different months, revealing the highest total energy consumption and output power in April and August, at 7,298.7 kW and 2.18×104 kW, respectively. Conversely, the lowest energy consumption and output power are observed in November and April, at 2,739.4 kW and 1.10×104 kW, respectively. The results indicate that the system's performance is significantly influenced by external environmental factors. Future research should investigate the system's performance and control strategies in various climatic regions across China, providing theoretical guidance for the application of solar energy and heat recovery in the environmental regulation of sow houses.

Keywords: Energy utilization efficiency; PV/T; Heat recovery; Operating parameters; Environmental regulation of sow houses

1 Introduction

As the global population continues to grow, the demand for livestock products, such as pork, has seen a sharp increase [1, 2]. However, numerous challenges, including improved pig productivity, reduced energy costs, and ensuring the health and safety of workers in pig houses, must be addressed. Regulating the thermal environment of pig houses is vital for enhancing productivity and economic benefits [3–5]; however, the energy and costs associated with temperature regulation systems are substantial [6, 7]. Furthermore, greenhouse gas emissions produced by temperature regulation systems in pig houses exacerbate global climate change [8, 9]. Therefore, the development of green and energy-efficient environmental regulation systems in pig houses is essential for sustainable growth [10].

In recent years, pig house environmental regulation systems have primarily included mechanical ventilation systems, ground source heat pump systems, and evaporative cooling systems [11–13]. Nevertheless, issues such as inadequate cooling effects and considerable investments must be addressed. Research has demonstrated that varying supply air speeds and directions in pig houses can effectively reduce energy consumption and greenhouse gas emissions. However, the cooling effect of ventilation systems is influenced by outdoor climate conditions. Compared to mechanical ventilation systems, greenhouse gas emissions and energy consumption were significantly reduced in pig houses with earth-tube heat exchangers. However, the cooling and heating effects of these systems require improvement. In pursuit of sustainable development, new green and energy-saving systems have been developed for pig houses. Studies have shown that energy consumption and greenhouse gas emissions are considerably reduced in pig houses with ground source heat pump systems, though high initial investments and limitations imposed by outdoor climatic conditions and geographical environments persist.

Evaporative cooling systems are commonly employed in pig houses to reduce indoor temperatures during hot seasons, improving the indoor thermal environment, pig welfare, and economic benefits. However, these systems increase relative humidity in pig houses, which in turn limits their cooling effect [4]. Consequently, the effectiveness of evaporative cooling systems is closely related to local humidity.

The utilization of solar energy has garnered widespread attention, but issues such as high initial investments and suitability for heating pig houses only during the cold season remain. Moon et al. found that the application of solar heating systems in pig houses reduces greenhouse gas emissions by 15% and energy consumption by 15-31% compared to mechanical ventilation systems. Other studies have shown significant reductions in energy consumption and greenhouse gas emissions in pig houses using heating systems based on solar energy and ground source heat pumps. However, the expensive initial investments and extended payback periods of solar heating systems hinder their widespread implementation in pig houses.

Research has indicated that heat recovery technology holds great potential for reducing operating costs and greenhouse gas emissions in pig houses. In this context, the combination of evaporative cooling systems with solar dehumidification and heat recovery could significantly improve cooling efficiency and reduce energy consumption. Nevertheless, research on the construction and operation control of such systems remains scarce. Therefore, developing and analyzing such systems is necessary to provide theoretical guidance for the application of solar energy and heat recovery technology in the environmental regulation of sow houses.

To enhance energy utilization efficiency and economic benefits in sow houses, this study proposes a novel annual temperature regulation system based on heat recovery and photovoltaic-thermal technology. The mathematical models of the key components in the new system are established and validated using literature data. Additionally, a numerical simulation is employed to analyze the system's operating characteristics across different months.

2 System Construction

A diagrammatic sketch of the newly proposed annual temperature regulation system based on heat recovery and photovoltaic-thermal technology for sow houses is presented in Figure 1. This system primarily consists of a grid-connected photovoltaic power generation system, a solar thermal system, and a supply and exhaust air regulation system. Key components include a PV/T collector, phase-change heat storage tank, phase-change heat exchanger, auxiliary electric heater, rotary dehumidifier, heat recovery device, sprinkler, and wet scrubber.

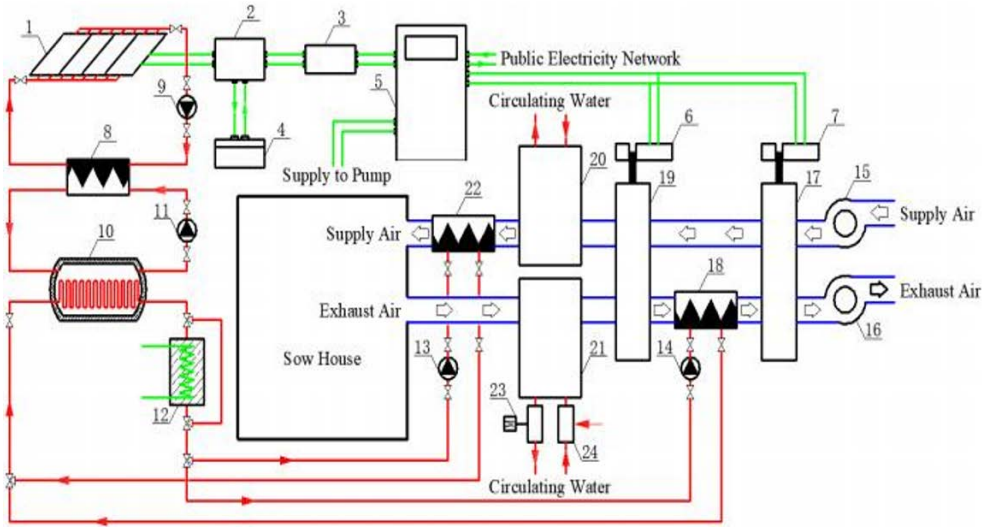

Figure 1. Diagrammatic sketch of a new annual temperature regulation system based on heat recovery and photovoltaic-thermal in sow houses

The red, green and blue lines represent water, circuit and air routes, respectively. 1. PV/T collectors. 2. Photovoltaic controller. 3. Photovoltaic inverter. 4. Battery. 5. AC distribution cabinet. 6. The first drive motor. 7. The second drive motor. 8. Phase-change heat exchanger. 9. The first hot water circulating pump. 10. Phase-change heat storage tank. 11. The second hot water circulating pump. 12. Auxiliary electric heater. 13. The first cold water circulating pump. 14. The second cold water circulating pump. 15. Supply fan. 16. Exhaust fan. 17. Rotary dehumidifier. 18. The first air-water heat exchanger. 19. Heat recovery device. 20. Sprinkler. 21.Acid scrubber. 22. The second air-water heat exchanger. 23. Conductivity detector. 24. sulfuric acid and organic solvents adding device.

In the grid-connected photovoltaic power generation system, solar energy is converted into DC by photovoltaic modules on the PV/T collector, which is then transmitted to a photovoltaic controller. The DC is subsequently converted into AC by a photovoltaic inverter, and, after voltage regulation, is distributed to the first and second drive motors through an AC distribution cabinet. These motors drive the heat recovery device and rotary dehumidifier, enabling supply air dehumidification and exhaust air heat recovery. Additionally, voltage-regulated AC powers the circulating water pump and heats the circulating water within the system. Excess solar energy is stored in a battery through the photovoltaic controller, and once the battery is fully charged, it can be sold to the public electricity

network via the AC distribution cabinet. When solar energy is insufficient to meet the power demands of the sow houses, the new system is directly supplied by the public electricity network through the AC distribution cabinet.

The solar thermal system functions by circulating water that absorbs solar heat through the PV/T collector and is transported by the first hot water circulating pump. This water then exchanges heat with the working medium on the opposite side of the phase-change heat exchanger. The heated working medium is subsequently transported to the phase-change heat storage tank by the second hot water circulating pump, where phase-change material stores the heat. Once the circulating water on the other side of the phase-change heat storage tank absorbs the heat of the phase-change material, it is heated by the first air-water heat exchanger via the circulating pump. The circulating water is heated through the second air-water heat exchanger when supply air in the sow house requires heating. If the heat from the phase-change material is inadequate to meet the heat demand, additional heat is supplied by the auxiliary electric heater.

The supply and exhaust air regulation system begin with sow house exhaust air entering an acid scrubber, where it is washed with sulfuric acid and organic solvent to remove odor gases. The resulting wastewater can be used for crop irrigation once its pH value is determined by a conductivity detector. The exhaust air then enters the heat recovery device to exchange heat with the supply air. When dehumidification of supply air is necessary, exhaust air is heated by circulating water and directed through the rotary dehumidifier before being discharged by an exhaust fan. If dehumidification is not required, exhaust air is directly expelled into the atmosphere via the exhaust fan. On the supply air side, air is first dehumidified in the rotary dehumidifier before entering the heat recovery device to exchange heat with exhaust air. Supply air is cooled by spray water and sent into the sow house if its temperature exceeds the set value, whereas, if the temperature is below the set value, supply air is heated through the second air-water heat exchanger before being introduced into the sow house.

Table 1. Some design and operation parameters of new system

NO.	Item	Value	Unit	NO.	Item	Value	Unit
1	Inlet temperature of PV/T collector	45	$^{\circ}\mathrm{C}$	9	Set inlet humidity of the rotary dehumidifier	70	$\%$
2	Mass flow rate of $\mathrm{PV/T}$ collector	6000	$\mathrm{kg/h}$	10	Fan power	682.8	kW
3	Area of PV/T collector	878	m^2	11	Set inlet low/high temperature of heat recovery device in cooling season	$18/26$	$^{\circ}\mathrm{C}$
4	Slope of PV/T collector	30	$\circ$	12	Set inlet low/high temperature of heat recovery device in heating season	$20/26$	$^{\circ}\mathrm{C}$
5	Mass flow rate of supply air	33150	$\mathrm{m}^{3/h}$	13	Efficiency ofheat recovery device Set inlet temperature of second cold water	85	$\%$
6	Pump power	745.6	kW	14	Circulating pump in the cooling/heating season	$18/24$	$^{\circ}\mathrm{C}$
7	Inlet/outlet temperature of phase-change heat storage tank	$55/75$	$^{\circ}\mathrm{C}$	15	Set inlet temperature of sprinkler in cooling/heating season	$22/26$	$^{\circ}\mathrm{C}$
8	Volume of phase-change heat storage tank	15	m^3	16	Area of sow house	219	m^2

Table 2. Four operating modes of new system

Mode	Outdoor Climate Conditions	Specific Description
Mode 1	Abundant solar energy resources	The heat converted by solar energy is used to dehumidify the exhaust air or heat the supply air; The surplus heat is used for heat storage.
Mode 2	Sufficient solar energy resources	The heat converted by solar energy is used to dehumidify the exhaust air or heat the supply air.
Mode 3	Lack of solar energy resources	The heat converted by solar energy and stored in the phase-change heat storage tank is used to dehumidify the exhaust air or heat the supply air; When the heat supply of phase-change material cannot meet the heat demand of sow house, the additional heat is provided by auxiliary heater. The heat stored in the phase-change heat storage tank is used to dehumidify the exhaust air or heat.
Mode 4	Rainy day or night	The supply air; When the heat supply of phase-change material cannot meet the heat demand of sow house, the additional heat is provided by auxiliary heater.

Table 1 presents design and operational parameters of the new system, while Table 2 outlines its four operating modes, which are determined by outdoor climate conditions. In summary, the main advantages of the novel system include: (1) reduced energy consumption and associated costs through the use of heat recovery and photovoltaic-

thermal technology; (2) suitability for annual temperature regulation in high-humidity regions, leading to improved evaporative cooling efficiency and enhanced sow productivity and welfare; and (3) heat recovery and deodorization of exhaust air, resulting in increased energy utilization efficiency and reduced greenhouse gas emissions.

3 Mathematical Models of Key Equipment

The new system primarily consists of a rotary dehumidifier, PV/T collector, and phase-change heat storage tank, among other components. To effectively simulate the new system, mathematical models are established for its key equipment according to TRNSYS. The modeling process is described as follows:

3.1 Rotary Dehumidifier

The rotary dehumidifier model is established based on type 1716 in TRNSYS as Figure 2, with silica gel serving as the desiccant material. The following assumptions are made: (1) a one-dimensional analysis that neglects heat and mass transfer in the radial and circumferential directions of the rotor; (2) a rotor fabricated as a honeycomb structure with equal shape and size for air channels; (3) a uniformly distributed rotor with constant thermal properties for its materials; (4) constant heat and mass transfer coefficients between air and desiccant wall; (5) adiabatic air channels; (6) neglect of thermal and hygroscopic capacitance effects.

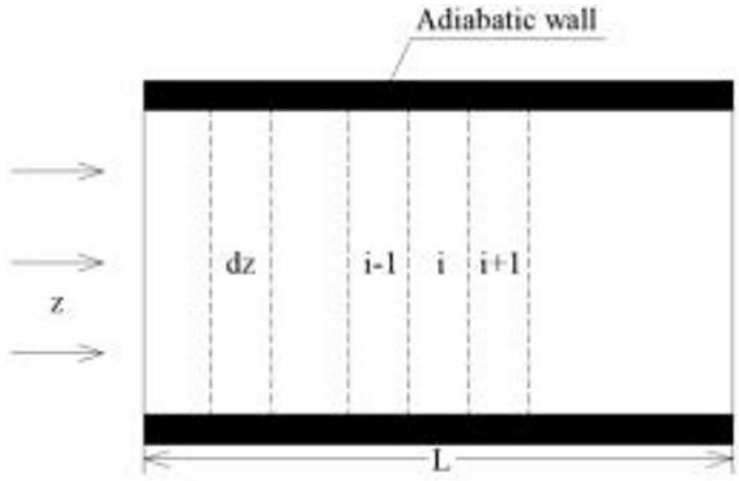

Figure 2. One dimensional micro-element model of rotary dehumidifier

The perimeter L_{p} and cross-sectional area A of air channels are as follows:

$$L_{\mathrm{p}} \approx 2b + 2\sqrt{b^2 + (a\pi)^2}\left[\frac{3 + (2b/a\pi)^2}{4 + (2b/a\pi)^2}\right] \tag{1}$$

where, $A = 2ab$; a and b are the half height and width of air channels, respectively.

The mass balance between desiccant wall and air is as follows:

$$\frac{\partial Y}{\partial t} + V\frac{\partial Y}{\partial z} + \omega_1\frac{\partial W}{\partial t} = 0 \tag{2}$$

where, T is air absolute temperature; Y is the humidity ratio of wet air; W is the moisture content of silica gel.

$$\omega_1 = \frac{f_{\mathrm{d}}}{2A\rho_{\mathrm{a}}} \tag{3}$$

The mass transfer equation of desiccant wall is as follows:

$$\frac{\partial W}{\partial t} + \omega_2\left(Y_{\mathrm{w}} - Y\right) = 0 \tag{4}$$

where, Y_{W} is the humidity ratio of isothermal wet air containing desiccant material.

$$\omega_2 = \frac{2K_{\mathrm{y}}P}{f_{\mathrm{d}}} \tag{5}$$

The energy balance between air and desiccant wall is as follows:

$$\frac{\partial T}{\partial t}+V\frac{\partial T}{\partial z}+\omega_3\frac{\partial T^*}{\partial t}=\omega_4\left(Y-Y_{\mathrm{w}}\right) \tag{6}$$

where, *V* is air flow velocity; T^* is the absolute temperature of silica gel.

$$\omega_3=\frac{f_{\mathrm{d}}\left(c_{\mathrm{pd}}+Wc_{\mathrm{w}}\right)+f_{\mathrm{m}}c_{\mathrm{pm}}}{2A\rho_{\mathrm{a}}\left(c_{\mathrm{pa}}+Yc_{\mathrm{pv}}\right)} \tag{7}$$

$$\omega_4=\frac{K_{\mathrm{y}}P\Delta H_{\mathrm{a}}}{A\rho_{\mathrm{a}}\left(c_{\mathrm{pa}}+Yc_{\mathrm{pv}}\right)} \tag{8}$$

where, f_{d} and f_{m} are the mass of silica gel and matrix material per unit length, respectively, $\mathrm{kg/m}$; $c_{\mathrm{pd}}, c_{\mathrm{w}}, c_{\mathrm{pm}}, c_{\mathrm{pa}}$ and c_{pv} are the specific heat capacity of silica gel, water, matrix material, air and water vapor, respectively, kJ/(kg K); $P\mathrm{a}$ is air density, $\mathrm{kg/m^3}$; $\mathrm{K_y}$ is the mass transfer coefficient between air and silica gel, $\mathrm{kg/\left(m^2\ s\right)}$; P is wheel pressure, kPa; ΔH_{a} is the adsorption heat of silica gel, kJ/kg.

The heat transfer equation of desiccant wall is as follows:

$$\frac{\partial T^*}{\partial t}+\omega_5\left(T^*-T\right)+\omega_6\left(Y_{\mathrm{w}}-Y\right)+\omega_7\left(Y_{\mathrm{w}}-Y\right)\left(T-T^*\right)=0 \tag{9}$$

$$\omega_5=\frac{2hL_{\mathrm{p}}}{f_{\mathrm{d}}\left(c_{\mathrm{pd}}+Wc_{\mathrm{w}}\right)+f_{\mathrm{m}}c_{\mathrm{pm}}} \tag{10}$$

$$\omega_6=\frac{2K_{\mathrm{y}}\Delta H_{\mathrm{a}}}{f_{\mathrm{d}}\left(c_{\mathrm{pd}}+Wc_{\mathrm{w}}\right)+f_{\mathrm{m}}c_{\mathrm{pm}}} \tag{11}$$

$$\omega_7=\frac{2K_{\mathrm{y}}Pc_{\mathrm{pv}}}{f_{\mathrm{d}}\left(c_{\mathrm{pd}}+Wc_{\mathrm{w}}\right)+f_{\mathrm{m}}c_{\mathrm{pm}}} \tag{12}$$

$$h=\frac{Nu_{\mathrm{a}}k_{\mathrm{a}}L_{\mathrm{p}}}{4A} \tag{13}$$

$$K_{\mathrm{y}}=\rho_{\mathrm{a}}\frac{Sh_{\mathrm{a}}DL_{\mathrm{p}}}{4A} \tag{14}$$

$$D=\frac{2.256}{P_{\mathrm{a}}}\left(\frac{T_{\mathrm{a}}+273.13}{256}\right)^{1.81} \tag{15}$$

where, *h* is the heat transfer coefficient, $\mathrm{w/\left(m^2\ K\right)}$; Nu_{a} is Nusselt number; k_{a} is air thermal conductivity, W/(mK); is Sherwood number; *D* is the diffusion coefficient of water vapor, $\mathrm{m^2/s}$; p_{a} is air pressure, kPa; T_{a} is air temperature, ℃.

According to the literature [14], the adsorption heat of silica gel is as follows:

$$Q=h_{\mathrm{v}}\left(1.0+0.2843\mathrm{e}^{-10.28W}\right) \tag{16}$$

where, h_{v} is the latent heat of water evaporation, J/kg.

The correlation between humidity and relative humidity is as follows:

$$Y_{\mathrm{w}}=\frac{0.62188\phi_{\mathrm{w}}}{p_{\mathrm{atm}}/p_{\mathrm{ws}}-\phi_{\mathrm{w}}} \tag{17}$$

where, φ_{w} is the relative humidity of silica gel, %; p_{ws} is the saturated water vapor pressure, kPa.

According to the literature [15], φ_w and p_{ws} can be obtained as follows:

$$\phi_{\mathrm{w}}=0.0078-0.05759W+24.16554W^2-124.78W^3+204.226W^4 \tag{18}$$

The saturated vapor pressure of water is determined by the Antonine equation, as shown as follows:

$$p_{\mathrm{ws}} = \exp\left(23.196 - \frac{3816.44}{T^* - 46.13}\right) \tag{19}$$

The energy transferred by rotary dehumidifier to process air can be calculated as follows:

$$q_{\text{fresh}} = m_{\text{fresh}} \left(h_{\text{out,fresh}} - h_{\text{in,fresh}}\right) \tag{20}$$

where, q_{fresh} is the absorption of heat from process air, J/s; $h_{\text{out, fresh}}$ is the outlet enthalpy value of process air, J/kg; $h_{\text{in, fresh}}$ is the inlet enthalpy value of process air, J/kg; m_{fresh} is the mass flow rate of process air, kg/s.

The amount of water removed from the air of rotary dehumidifier can be calculated as follows:

$$W_{\text{fresh}} = m_{\text{fresh}} \left(\omega_{\text{out,fresh}} - \omega_{\text{in,fresh}}\right) \tag{21}$$

where, W_{fresh} is the dehumidification capacity of process air, g/s; $\Phi_{\text{out,fresh}}$ is the outlet moisture content of process air, g/kg; $\Phi_{\text{in,fresh}}$ is the inlet moisture content of process air, g/kg.

The outlet conditions of regeneration air can be calculated as follows:

$$h_{\text{out, regen}} = h_{\text{in,regen}} - \frac{q_{\text{regen}}}{m_{\text{regen}}} \tag{22}$$

where, q_{regen} is the heat absorbed by regeneration air, J/s; $h_{\text{out,regen}}$ is the outlet enthalpy value of regeneration air, J/kg; $h_{\text{in,regen}}$ is the inlet enthalpy value of regeneration air, J/kg; m_{regen} is the mass flow rate of regeneration air, kg/s.

3.2 PV/T Collector

The specific structure of the PV/T collector is depicted in Figure 3. Disregarding energy conduction along the surface of the photovoltaic panel, the energy balance equation is established at any point on the panel's surface, as shown in the following equation:

$$S - h_{\text{out}} \left(T_{\mathrm{PV}} - T_{\mathrm{amb}}\right) - h_{\mathrm{rad}} \left(T_{\mathrm{PV}} - T_{\mathrm{sky}}\right) - \frac{T_{\mathrm{PV}} - T_{\mathrm{abs}}}{R_{\mathrm{T}}} = 0 \tag{23}$$

where, S is the net absorbed solar radiation per unit area, $\mathrm{W/m^2}$; h_{out} is the convection heat transfer coefficient with the surrounding environment, W/($\mathrm{m^2}$ ℃); T_{PV} is the temperature of photovoltaic panel, ℃; T_{amb} is the ambient temperature, ℃; h_{rad} is the radiation heat transfer coefficient, W/($\mathrm{m^2}$ ℃); T_{sky} is the sky temperature, ℃; T_{abs} is the temperature of heat absorbing panel, ℃; R_{T} is the thermal resistance of material between the photovoltaic panel and the heat absorbing panel, $\mathrm{m^2}$ ℃/W. The radiation heat transfer coefficient h_{rad} can be obtained by the following equation:

$$h_{\mathrm{rad}} = \varepsilon\sigma \left(T_{\mathrm{PV}} + T_{\mathrm{sky}}\right)\left(T_{\mathrm{PV}}^2 + T_{\mathrm{sky}}^2\right) \tag{24}$$

where, σ is Stephen Boltzmann constant, taken as 5.67×10^{-8} $\mathrm{W/m^2{\circ}C^4}$; ε is the surface radiation coefficient of photovoltaic panel, taken as 0.9. S can be obtained by subtracting the photovoltaic power generation from the total solar radiation absorbed by photovoltaic panel, as shown in the following equation:

$$S = (\tau\alpha)_{\mathrm{n}} LAMG_{\mathrm{T}} \left(1 - \eta_{\mathrm{PV}}\right) \tag{25}$$

where, $(\tau a)_n$ is the effective projected absorption product of direct light under normal incidence, taken as 0.85; *IAM* is the correction coefficient of incident angle, taken as 0.1; G_{T} is the total solar radiation, $\mathrm{W/m^2}$; η_{PV} is photovoltaic efficiency, %. The photovoltaic efficiency is related to the temperature and the incident solar radiation of the photovoltaic panels, as follows:

$$\eta_{\mathrm{PV}} = \eta_{\text{nominal}} X_{\text{Cell Temp}} X_{\text{Radiation}} \tag{26}$$

where, η_{nominal} is the photovoltaic efficiency under standard test conditions (STC), %; X_{celltemp} is the function of silicon cell efficiency and cell temperature; $X_{\text{radiation}}$ is the function of silicon cell efficiency and incident radiation.

$$X_{\text{Cell temp}} = 1 + Eff_{\mathrm{T}} \left(T_{\mathrm{PV}} - T_{\text{ref}}\right) \tag{27}$$

where, T_{ref} is the reference temperature under STC, taken as 25℃; Eff_{T} is the silicon cell efficiency under the reference temperature.

$$X_{\text{Radiation}} = 1 + Eff_{\mathrm{G}} \left(G_{\mathrm{T}} - G_{\text{ref}}\right) \tag{28}$$

where, G_{ref} is the reference spectral irradiance under STC, taken as $1000\ W/m^2$; E_{ffG} is the silicon cell efficiency under the reference spectral irradiance. After the photovoltaic efficiency is obtained according to Eqs. (27)-(29), the output electric power under the effective areas can be further obtained by the following equation:

$$\text{Power } = (\tau\alpha)_n\, IAMG_T A_{PVT}\eta_{PV} \tag{29}$$

where, APV/T is the area of PV/T collector, m^2.

After the working medium absorbs the heat from the heat absorbing panel, the outlet temperature of PV/T collector can be obtained by the following equation:

$$T_{\text{fluid,in}} = \left(T_{\text{fuild,in}} + \frac{\varepsilon}{k}\right)\exp\left(\frac{N_{\text{tubes}}}{mC_{ps}}\frac{k}{\theta}L\right) - \frac{\varepsilon}{k} \tag{30}$$

where, $T_{\text{fluid,out}}$ is the outlet temperature of PV/T collector, ℃; $T_{\text{fluid,in}}$ is the inlet temperature of PV/T collector, ℃; N_{tubes} is the number of channels after the heat absorption plate; C_{ps} is the specific heat flowing the fluid through PV/T collector, kJ / (kg ℃); L_{pv} is the length of PV/T collector along the fluid direction.

The heat absorbed by PV/T collector can be calculated by the following equation:

$$Q_u = mC_p\left(T_{\text{fluid,out}} - T_{\text{fluid,in}}\right) \tag{31}$$

$$\eta_t = \frac{Q_u}{S} \tag{32}$$

where, η_t is the thermal efficiency of PV/T collector, %; Q_u is the heat collector of PV/T collector, kJ.

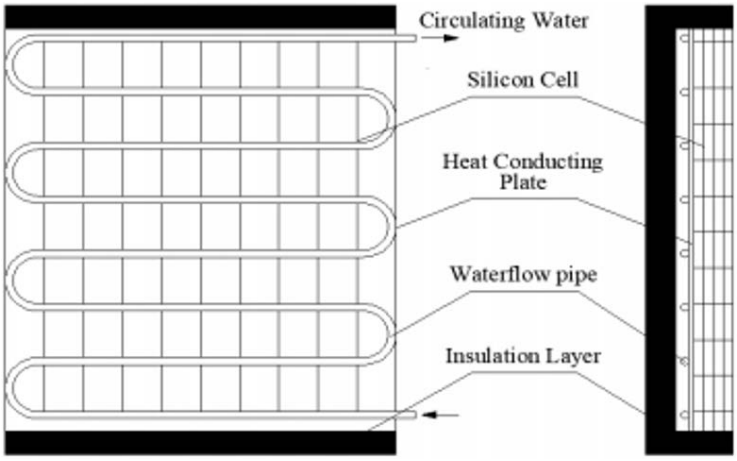

Figure 3. Specific structure of PV/T collector

3.3 Phase-Change Heat Storage Tank

The phase-change heat storage tank model is established according to type 1334 in the TRNSYS database. To solve the heat transfer process of the phase-change heat storage tank, the following assumptions are made: (1) The phase-change material is single and isotropic, and its phase change occurs within a specific temperature range; (2) The heat transfer coefficients are constant between the inner surface of the phase-change heat storage tank and water, as well as between the outer surface of the phase-change heat storage tank and outside air; (3) The equivalent specific heat capacity of the phase-change material is the mean value of the specific heat capacity of pure solid and liquid in the phase-change process; (4) The vertical convection heat transfer is considered between the phase-change material and water. The enthalpy of paraffin is calculated as follows:

$$h = c_p\left(T_s - 273.15\right) + H \tag{33}$$

where, c_p is the specific heat capacity of phase-change material in the actual heat transfer process, kJ/(kg K); *H* is the latent heat in the actual phase-change process, kJ/kg; T_S is the temperature of phase-change material in the actual process, K.

According to the principle of energy conservation, the heat absorbed on the surface of the phase-change material is equal to the heat stored by the phase-change material in the form of latent heat plus the heat transfer between the

phase change material and the adjacent interface. The heat transfer correlation of the phase-change material is as follows:

$$\frac{\lambda_{\mathrm{s}}}{r}\frac{\partial}{\partial r}\left(r\frac{\partial T}{\partial r}\right)=\rho_{\mathrm{s}}C_{\mathrm{p}}\frac{\partial T(r,t)}{\partial t} \tag{34}$$

where λ_s is the thermal conductivity of phase-change material, W/(m K); r is the distance from the central axis of TANK, m; p is the density of phase-change material, $\mathrm{kg/m^3}$.

The two-dimensional heat transfer model of phase-change material is established by enthalpy method and the heat transfer equation is as follows:

$$\frac{\alpha h}{\alpha t}+v_{\mathrm{y}}\frac{\alpha h}{\alpha y}=\frac{\partial}{\partial y}\left(\lambda\frac{\partial T}{\partial y}\right)+\frac{1}{r}\frac{\partial}{\partial r}\left(r\cdot\lambda\frac{\partial T}{\partial r}\right) \tag{35}$$

where, v_{y} is the vertical velocity of phase-change material under the action of gravity, m/s.

There are primarily three modes of heat exchange in the phase-change heat storage tank: (1) the heat exchange between the fluid in the tank and the fluid in the heat exchanger through immersion heat transfer; (2) the heat exchange between the fluid in the environment and the tank; and (3) the interactive heat exchange between the fluid in the tank and the fluid flowing into and out of the tank. The thermal balance equation of the phase-change heat storage tank is as follows:

$$\frac{dT_{\text{Tank}}}{dt}=\frac{Q_{\text{in, Tank}}-Q_{\text{out, Tank}}}{C_{\text{Tank}}} \tag{36}$$

where, Q_{in} , Tank and Q_{out} , Tank are the heat transfer rate of fluid at the inlet and outlet of tank, respectively, kJ/h; C_{Tank} is the mean specific heat capacity of fluid in tank.

According to the above analysis, the above equation can be further expressed as follows:

$$\frac{dT_{\text{Tank}}}{dt}=\frac{Q_{\text{flow}}+Q_{\text{hx}}-Q_{\text{loss, top}}-Q_{\text{loss, bottom}}-Q_{\text{loss, edges}}}{C_{\text{Tank}}} \tag{37}$$

where, Q_{flow} is the heat transfer rate of the fluid into tank, kJ/h; Q_{hx} is the heat transfer rate of fluid flowing into the heat exchanger, kJ/h; Q_{loss} , top, Q_{loss} , bottom and Q_{loss} , edges are the heat transfer rate between tank and the ambient temperature at the top, edges and bottom of tank, respectively, kJ/h.

The heat transfer rate of fluid flowing into tank can be obtained by the following equation:

$$Q_{\text{flow}}=m_{\text{tank,in}}\,C_{\text{p, fluid}}\,(T_{\text{in,tank}}-T_{\text{tank}}) \tag{38}$$

where, $m_{\text{tank ,in}}$ is the mass flow rate of fluid flowing into tank, kg/h; $c_{\text{p, fluid}}$ is the specific heat capacity of fluid in the tank, kJ/(kg K); $T_{\text{in,tank}}$ is the temperature of fluid flowing into tank, ℃; Ttank is the mean temperature of tank, ℃.

The heat transfer rate of fluid flowing into the immersed heat exchanger can be obtained by the following equation:

$$Q_{\mathrm{hx}}=Eff_{\mathrm{hx}}*m_{\mathrm{hx,in}}C_{\mathrm{p,hx}}\,(T_{\mathrm{in,hx}}-T_{\mathrm{tank}}) \tag{39}$$

where, Eff_{hx} is the heat transfer efficiency of heat exchanger; $m_{\mathrm{hx,in}}$ is the mass flow rate of fluid flowing into the heat exchanger, kg/h; $c_{\mathrm{p,hx}}$ is the specific heat capacity of fluid in the heat exchanger, kJ/(kg·K); $T_{\mathrm{in,hx}}$ is the temperature of fluid flowing into the heat exchanger, ℃.

When there is no flow through the heat exchanger, there is no heat transfer from the heat exchanger. The outlet temperature from the heat exchanger can be expressed as follows:

$$T_{\text{out,hx}}=T_{\text{in,hx}}-\frac{Q_{\mathrm{hx}}}{m_{\mathrm{hx,in}}C_{\mathrm{p,hx}}} \tag{40}$$

where, $T_{\text{out,hx}}$ is the fluid temperature flowing out the heat exchanger, ℃ .

The heat transfer rate between tank and the ambient temperature at the top, edges and bottom of tank can be obtained by the following equation:

$$\begin{cases} Q_{\text{loss, top}}=A_{\text{top}}\,U_{\text{top}}\,(T_{\text{tank}}-T_{\text{env, top}}) \\ Q_{\text{loss, bottom}}=A_{\text{bottom}}\,U_{\text{bottom}}\,(T_{\text{tank}}-T_{\text{env, bottom}}) \\ Q_{\text{loss, edges}}=A_{\text{edges}}\,U_{\text{edges}}\,(T_{\text{tank}}-T_{\text{env, edges}}) \end{cases} \tag{41}$$

where, A_{top} is the surface area at the top of tank $\mathrm{m^2}$; A_{bottom} is the surface area at the bottom of tank, $\mathrm{m^2}$; A_{edges} is the surface area at the edges of tank, $\mathrm{m^2}$; U_{top} is the heat loss coefficient at the top of tank; U_{bottom} is the heat loss coefficient at the bottom of tank; U_{edges} is the heat loss coefficient at the edges of tank; T_{env} , top is the ambient temperature at the top of tank, ℃; T_{env} , bottom is the ambient temperature at the bottom of tank, ℃; T_{env} , edges is the ambient temperature at the edges of tank, ℃.

4 Simulation Method and Model Validation

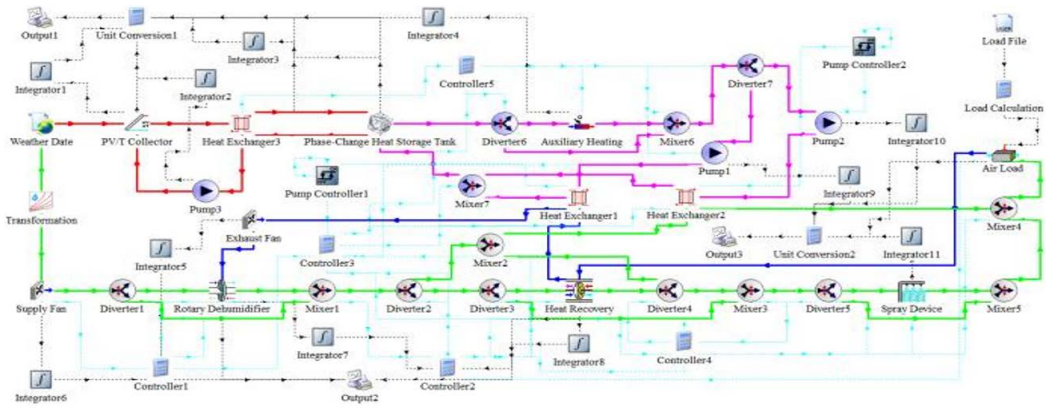

Figure 4. The model of new system based on TRNSYS18

Note: The red, green and blue solid lines represent water, supply and exhaust routes, respectively

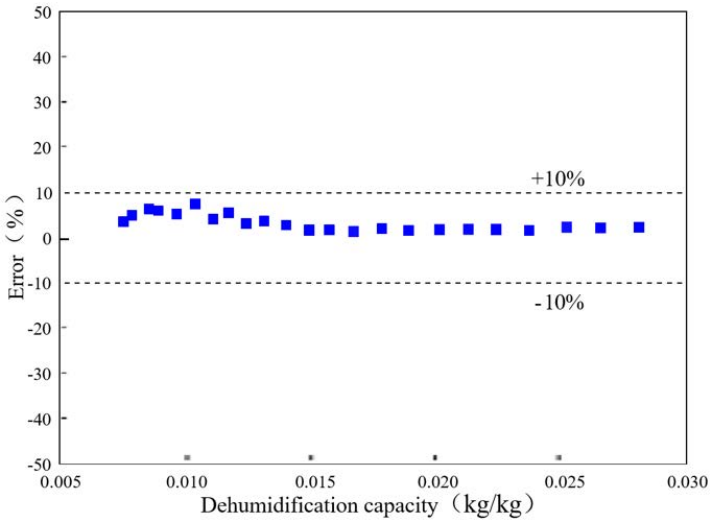

Figure 5. Comparison of dehumidification capacity calculated by simulation with that obtained by experiment

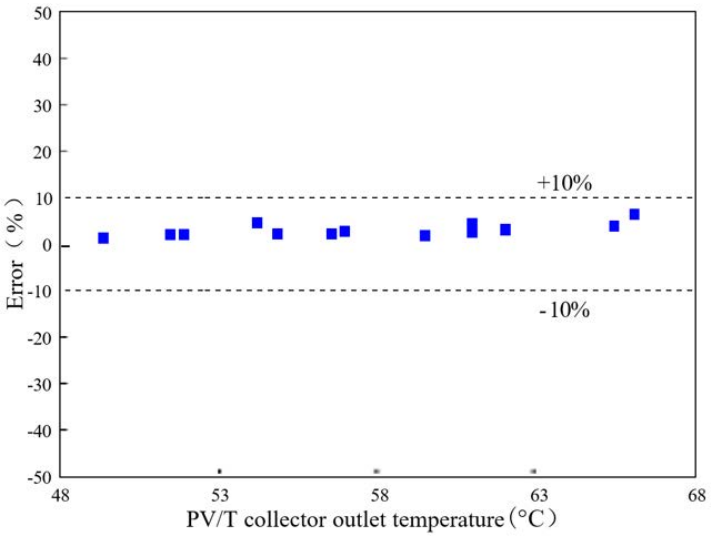

Figure 6. Comparison of the calculated data with the experimental datain the literature

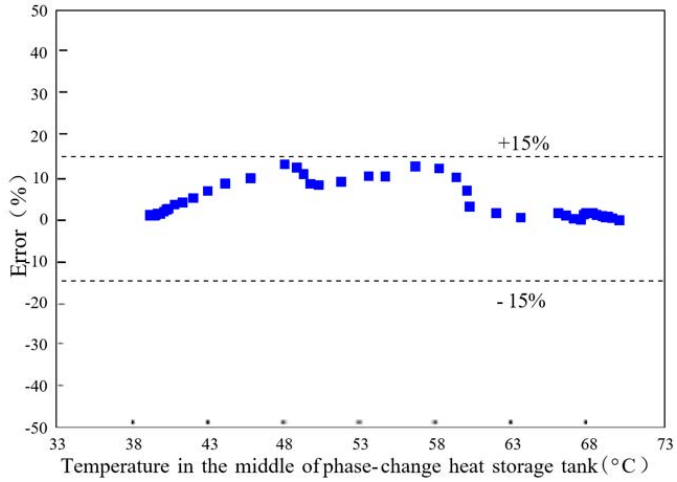

Figure 7. Comparison between the calculated data of model and the experimental data in the literature

Based on the analysis of the aforementioned models, TRNSYS18 was employed to establish the mathematical model of the new system in order to investigate its operational characteristics. Figure 4 illustrates the new system model developed using TRNSYS18. To ensure the accuracy of system simulation, the mathematical models of key equipment underwent further validation. Figure 5 presents the comparison of dehumidification capacity calculated by simulation with that obtained experimentally at various inlet temperatures. The results demonstrate that the maximum discrepancy between the simulated results and the experimental results is only 6.8%. Figure 6 displays the comparison of the calculated data with the experimental data from the literature. It was determined that the maximum error between the simulated results and the experimental results was only 6.78%. Figure 7 compares the calculated data of the model with the experimental data found in the literature. The results indicate that the mean and maximum errors of temperature in the middle of the phase-change heat storage tank are 3.9% and 14.48%, respectively. In summary, it can be concluded that the aforementioned models satisfy the simulation requirements and can be applied for the new system simulation.

5 Results and Discussion

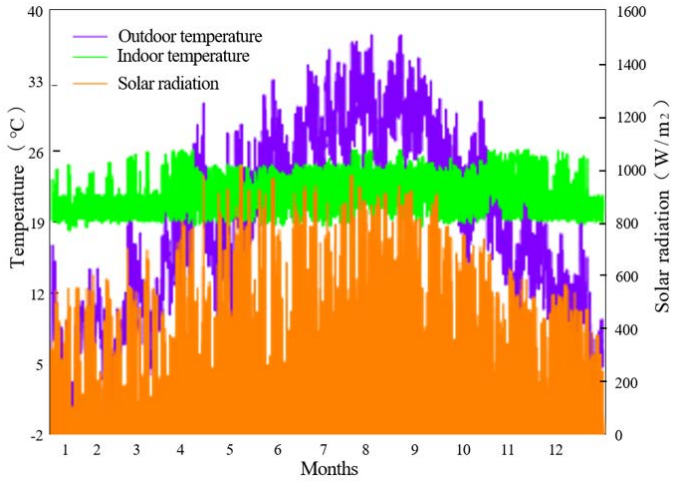

Figure 8. Outdoor dry bulb temperature regulated indoor temperature and solar radiation intensity received by the surface in Nanchang

Utilizing the system model, Nanchang was selected as a case study to simulate the operational characteristics of the new system. Figure 8 displays the outdoor dry bulb temperature, regulated indoor temperature, and solar radiation intensity received by the surface in Nanchang. The results reveal that the outdoor dry bulb temperature fluctuates between -2℃ and 40℃ throughout the year in Nanchang, while the indoor temperature is regulated within the range of 18-27℃ by the new system. Concurrently, it is observed that solar energy resources in Nanchang are relatively abundant from May to September, with an average of approximately 900 $\mathrm{W/m^2}$. Conversely, they are

relatively scarce from January to April and October to December, with an average of around 500 $\mathrm{W/m^2}$. Based on this analysis, the operational characteristics of the new system will be further examined in different months.

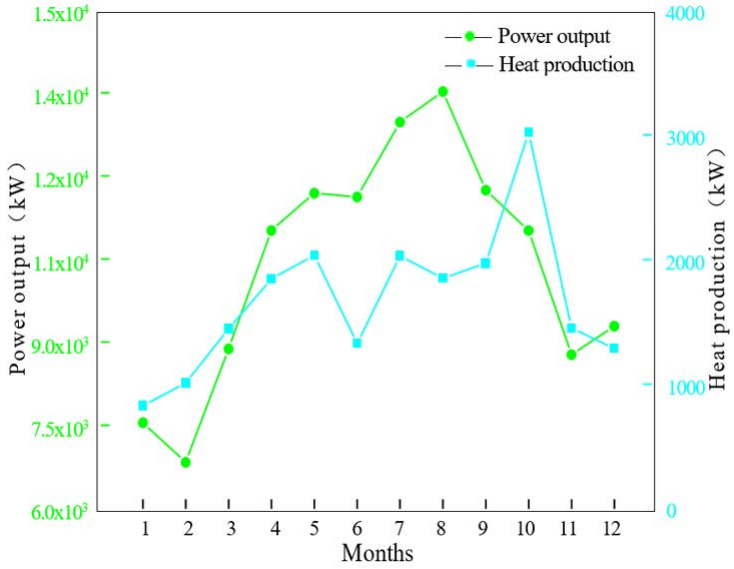

Figure 9. Change of annual power and heat production in the new system

Figure 9 illustrates the annual power and heat production changes in the new system. According to Figure 9, it is observed that the annual power and heat production of the new system are significantly influenced by outdoor environmental factors, with total values of 1.25×10^5 kW and 2.0×10^4 kW, respectively. Specifically, the power output of the PV/T collector increases from 6820.3 kW to 1.35×10^4 kW from February to August and decreases from 1.35×10^4 kW to 8763.2 kW from August to November. The heat production of the PV/T collector increases from 820.4 kW to 2025.8 kW from January to May, experiences a significant decrease in June, and then increases from 1319.6 kW to 3012.3 kW from June to October. From October to December, it decreases from 3012.3 kW to 1279.4 kW. In summary, the power output of the PV/T collector reaches its minimum and maximum values in February and August, at 6820.3 kW and 1.35×10^4 kW, respectively. Similarly, its heat production achieves the minimum and maximum values in January and October, at 820.42 kW and 3012.3 kW, respectively.

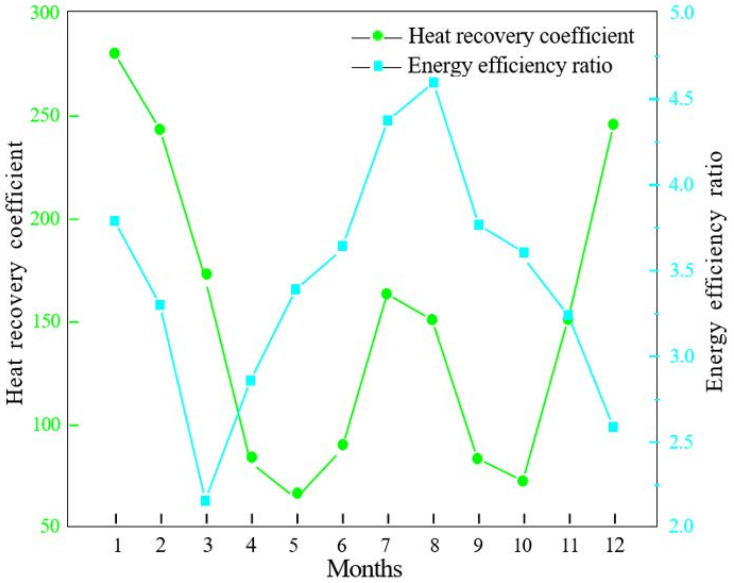

Figure 10. Change of annual heat recovery coefficient and energy efficiency ratio

Figure 10 presents the annual heat recovery coefficient (the ratio of the recovered heat to the power consumption of the heat recovery device) and energy efficiency ratio (the ratio of the cooling/heating capacity to the power consumption of cooling/heating equipment) changes. According to Figure 10, it is observed that the annual heat

recovery coefficient and energy efficiency ratio of the new system are significantly influenced by outdoor environmental factors, with mean values of 149.81 and 3.43, respectively. Specifically, the heat recovery coefficient decreases from 280.57 to 64.28 from January to May, increases from 64.28 to 163.74 from May to July, decreases from 163.74 to 72.76 from July to October, and then increases from 72.76 to 246.03 from October to December. In other words, the heat recovery coefficient reaches its minimum and maximum values in May and January, at 64.28 and 280.57, respectively. In addition, the energy efficiency ratio of the new system decreases from 3.79 to 2.16 from January to March, increases from 2.16 to 4.57 from March to August, and decreases from 4.57 to 2.59 from August to December. In other words, as time progresses, the energy efficiency ratio first decreases, then increases, and subsequently decreases. Specifically, it reaches its minimum and maximum values in March and August, at 2.16 and 4.57, respectively.

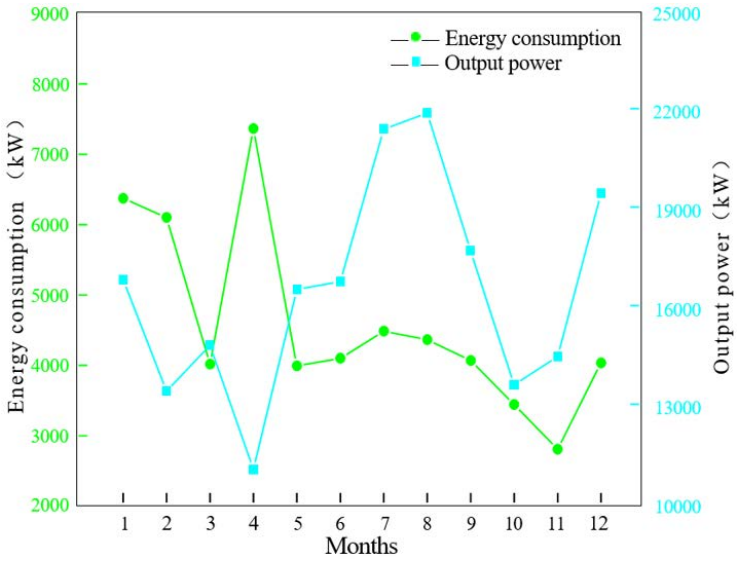

Figure 11. Change of annual operating energy consumption and output power of new system

Figure 11 displays the annual operating energy consumption and output power (the ratio of total output to total energy consumption) changes of the new system. According to Figure 11, it is observed that the annual operating energy consumption and output power of the new system are significantly influenced by outdoor environmental factors, with total values of 5.43×10^4 kW and 1.97×10^5 kW, respectively. The results demonstrate that the energy consumption reaches its minimum and maximum values in November and April, at 2739.4 kW and 7298.7 kW, respectively. Similarly, the output power of the new system achieves its minimum and maximum values in April and August, at 1.10×10^4 kW and 2.18×10^4 kW, respectively. This is attributed to the increased energy consumption of the auxiliary electric heater in January and April, while the heat recovery and cooling capacity of the new system are relatively high in July and August.

6 Conclusion

A novel annual temperature regulation system incorporating heat recovery and PV/T technologies has been proposed to enhance energy utilization efficiency and economic benefits in sow houses. Mathematical models for key equipment within the system were established and validated using data from existing literature, with a maximum error of less than 14.48%. A numerical simulation was employed to analyze the operational characteristics of the new system across different months. The main conclusions drawn from this study are as follows:

(1) The integration of heat recovery technology and PV/T technology in the proposed system successfully improved evaporative cooling efficiency and reduced energy consumption. The reliability of key equipment was ascertained through validation against literature data.

(2) It was found that the power output of the PV/T collector reached minimum and maximum values in February and August, with respective values of 6820.3 kW and 1.35×10^4 kW. Heat production from the PV/T collector was at its lowest in January (820.42 kW) and peaked in October (3012.3 kW). Heat recovery coefficients exhibited minimum and maximum values in May (64.28) and January (280.57), respectively. Energy efficiency ratios were lowest in March (2.16) and highest in August (4.57).

(3) Energy consumption was observed to be at its lowest in November (2739.4 kW) and highest in April (7298.7 kW). In contrast, the output power of the new system reached minimum and maximum values in April (1.10×10^4 kW) and August (2.18×10^4 kW), respectively. This can be attributed to the increased energy consumption of the auxiliary

electric heater in January and April, while the heat recovery and cooling capacity of the new system were relatively high in July and August.

(4) The operational parameters of the new system were significantly influenced by outdoor environmental factors. Future research should investigate the performance and control strategies of the new system for typical cities across the five climatic regions in China.

This study has provided valuable insights into the potential of the proposed annual temperature regulation system for sow houses, and paves the way for further optimization and implementation in a variety of climates.

Data Availability

The data used to support the findings of this study are available from the corresponding author upon request.

Conflicts of Interest

The authors declare that they have no conflicts of interest.

References

[1] F. A. O. Joint, "Food and agriculture organization of the United Nations," *Caramel Colours. Combined Compendium of Food Additive Specification, Monograph*, vol. 11, pp. 1817–7077, 2011.

[2] T. Fent, "Department of economic and social affairs, population division, United Nations expert group meeting on social and economic implications of changing population age structures," *Eur. J. Popul.*, vol. 24, pp. 451–452, 2008. https://doi.org/10.1007/s10680-008-9165-7

[3] J. S. Johnson, A. Sapkota, and D. C. Lay, "Rapid cooling after acute hyperthermia alters intestinal morphology and increases the systemic inflammatory response in pigs," *J. Appl. Physiol.*, vol. 120, no. 10, pp. 1249–1259, 2016. https://doi.org/10.1152/japplphysiol.00685.2015

[4] A. M. Williams, T. J. Safranski, D. E. Spiers, P. A. Eichen, E. A. Coate, and M. C. Lucy, "Effects of a controlled heat stress during late gestation, lactation, and after weaning on thermoregulation, metabolism, and reproduction of primiparous sows," *J. Anim. Sci.*, vol. 91, no. 6, pp. 2700–2714, 2013. https://doi.org/10.2527/jas.2012-6055

[5] J. S. Johnson, K. L. Martin, K. G. Pohler, and K. R. Stewart, "Effects of rapid temperature fluctuations prior to breeding on reproductive efficiency in replacement gilts," *J. Therm. Biol.*, vol. 61, pp. 29–37, 2016. https://doi.org/10.1016/j.jtherbio.2016.08.003

[6] A. Costantino, E. Fabrizio, A. Biglia, P. Cornale, and L. Battaglini, "Energy use for climate control of animal houses: The state of the art in europe," *Energy Procedia*, vol. 101, pp. 184–191, 2016. https://doi.org/10.1016/j.egypro.2016.11.024

[7] N. Kythreotou, G. Florides, and S. A. Tassou, "A proposed methodology for the calculation of direct consumption of fossil fuels and electricity for livestock breeding, and its application to Cyprus," *Energy*, vol. 40, no. 1, pp. 226–235, 2012. https://doi.org/10.1016/j.energy.2012.01.077

[8] L. D. Jacobson, D. R. Schmidt, W. F. Lazarus, and R. Koehler, "Reducing the environmental footprint of pig finishing barns," in *American Society of Agricultural and Biological Engineers*, 2011.

[9] B. Nakomcic-Smaragdakis, T. Stajic, Z. Cepic, and S. Djuric, "Geothermal energy potentials in the province of Vojvodina from the aspect of the direct energy utilization," *Renew. Sustain. Energy Rev.*, vol. 16, no. 8, pp. 5696–5706, 2012. https://doi.org/10.1016/j.rser.2012.05.038

[10] Q. Xie, J. Q. Ni, J. Bao, and Z. Su, "A thermal environmental model for indoor air temperature prediction and energy consumption in pig building," *Build. Environ.*, vol. 161, p. 106238, 2019. https://doi.org/10.1016/j.buildenv.2019.106238

[11] W. Faes, J. Maselyne, M. De Paepe, and S. Lecompte, "Modelling the energetic performance of a pig stable," in *ECOS 2021-The 34th International Conference on Efficiency, Cost, Optimization, Simulation and Environmental Impact of Energy System*, 2021.

[12] F. Hou, C. Shen, and Q. Cheng, "Research on a new optimization method for airflow organization in breeding air conditioning with perforated ceiling ventilation," *Energy*, vol. 254, p. 124279, 2022. https://doi.org/10.1016/j.energy.2022.124279

[13] Y. Kwak, H. Shin, M. Kang, S. H. Mun, S. K. Jo, S. H. Kim, and J. H. Huh, "Energy modeling of pig houses: A south korean feasibility study," *Energy Strategy Rev.*, vol. 36, p. 100672, 2021. https://doi.org/10.1016/j.esr.2021.100672

[14] J. Y. San, "Heat and mass transfer in a two-dimensional cross-flow regenerator with a solid conduction effect," *Int. J. Heat Mass Transf.*, vol. 36, no. 3, pp. 633–643, 1993. https://doi.org/10.1016/0017-9310(93)80039-W

[15] A. A. Pesaran and A. F. Mills, "Moisture transport in silica gel packed beds—I. Theoretical study," *Int. J. Heat Mass Transf.*, vol. 30, no. 6, pp. 1037–1049, 1987. https://doi.org/10.1016/0017-9310(87)90034-2

Nomenclature

A	-The cross-sectional area of air channels, m^2
A_{bottom}	-The surface area at the bottom of tank, m^2
A_{edges}	-The surface area at the edges of tank, m^2
$A_{\text{PV/T}}$	-The area of PV/T collector, m^2
A_{top}	-The surface area at the top of tank, m^2
AC	-Alternating current
a	-Half height of air channels, m
b	-Half width of air channels, m
C_{Tank}	-The mean specific heat capacity of fluid in the tank, kJ/(kg K)
c_{p}	-The specific heat capacity of phase-change material in the actual heat transfer process, kJ/(kg K)
c_{pa}	-The specific heat capacity of air, kJ/(kg K)
c_{pd}	-The specific heat capacity of silica gel, kJ/(kg K)
$c_{\text{p,fluid}}$	-The specific heat capacity of fluid in the tank, kJ/(kg •K)
$c_{\text{p,hx}}$	-The specific heat capacity of fluid in the heat exchanger, kJ/(kg •K)
c_{ps}	-The specific heat capacity of fluid, kJ/(kg K)
c_{pv}	-The specific heat capacity of water vapor, kJ/(kg K)
c_{w}	-The specific heat capacity of water, kJ/(kg K)
f_{d}	-The mass of silica gel per unit length, kg
f_{s}	-The proportion of the airflow area to the total cross-sectional area of wheel on the airflow section
f_{m}	-The mass of matrix material per unit length, m
f_{v}	-The surface area of adsorbent in the wheel per unit volume, $\mathrm{m}^2/\mathrm{m}^3$
G_{ref}	-The reference spectral irradiance under STC, W/m^2
G_{T}	-The total solar radiation, W/m^2
H	-The latent heat in the actual phase-change process, kJ/kg
$h_{\text{in,fresh}}$	-The enthalpy of supply air at the inlet of rotary dehumidifier, J/kg
$h_{\text{in,regen}}$	-The enthalpy of regeneration air at the inlet of rotary dehumidifier, J/kg
h_{out}	-The convection heat transfer coefficient with the surrounding environment, W/(m^2 ℃)
$h_{\text{out,fresh}}$	-The enthalpy of supply air at the outlet of rotary dehumidifier, J/kg
$h_{\text{out,regen}}$	-The enthalpy of regeneration air at the outlet of rotary dehumidifier, J/kg
h_{rad}	-The radiation heat transfer coefficient, W/(m^2 ℃)
h_{v}	-The latent heat of water evaporation, J/kg
ΔH_{a}	-The adsorption heat of silica gel, kJ/kg
K_y	-The mass transfer coefficient between air and silica gel, kg/(m^2 s)
L_p	-The perimeter of air channels, m
L_{pv}	-The length of PV/T collector along the fluid flow direction, m
m_{fresh}	-The mass flow rate of supply air, kg/s
$m_{\text{hx,in}}$	-The mass flow rate of fluid flowing into the immersed heat exchanger, kg/h
$m_{\text{tank,in}}$	-The mass flow rate of fluid flowing into tank, kg/h
m_{regen}	-The mass flow rate of regeneration air, kg/s
Nu_{a}	-Nusselt number
N_{tubes}	-The channel number behind the heat absorbing panel process, K
P	-Wheel pressure, kPa
P_{a}	-Air pressure, kPa
P_{ws}	-The saturated water vapor pressure, kPa
Q_{flow}	-The heat transfer rate of fluid flowing into tank, kJ/h
Q_{hx}	-The heat transfer rate of fluid flowing into the immersed heat exchanger, kJ/h
$Q_{\text{in,Tank}}$	-The heat transfer rate of fluid at the inlet of tank, kJ/h
$Q_{\text{loss,bottom}}$	-The heat transfer rate between tank and the ambient temperature at the bottom of tank, kJ/h
$Q_{\text{loss,edges}}$	-The heat transfer rate between tank and the ambient temperature at the edges of tank, kJ/h
$Q_{\text{loss,top}}$	-The heat transfer rate between tank and the ambient temperature at the top of tank, kJ/h
$Q_{\text{out,Tank}}$	-The heat transfer rate of fluid at the outlet of tank, kJ/h
Q_{u}	-The heat collection of PV/T collector, kJ
q_{fresh}	-The absorbed heat of supply air, J/s
$q_{\text{m,a}}$	-The mass flow rate of air per unit cross-sectional area of wheel, kg/(m^2 s)
q_{regen}	-The absorbed heat of regeneration air, J/s

r	-The distance from the central axis of tank, m
R_{T}	-The thermal resistance of material between the photovoltaic panel and the heat absorbing panel, m^2 ℃/W
Re	-Reynolds number
RH_{set}	-Set inlet relative humidity of rotary dehumidifier, %
S	-The net absorbed solar radiation per unit area, W/m^2
Sh_{a}	-Sherwood number
T	-The absolute temperature of air, K
T_{a}	-Air temperature, ℃
T_{abs}	-The temperature of heat absorbing panel, ℃
T_{amb}	-Ambient temperature, ℃
$T_{\mathrm{env,bottom}}$	-The ambient temperature at the bottom of tank, ℃
$T_{\mathrm{env,edges}}$	-The ambient temperature at the edges of tank, ℃
$T_{\mathrm{env,top}}$	-The ambient temperature at the top of tank, ℃
T_{exhaust}	-Exhaust air temperature, ℃
$T_{\mathrm{fluid,in}}$	-The inlet temperature of PV/T collector, ℃
$T_{\mathrm{fluid,out}}$	-The outlet temperature of PV/T collector, ℃
$T_{\mathrm{in,hx}}$	-The temperature of fluid flowing into the heat exchanger, ℃
$T_{\mathrm{in,tank}}$	-The temperature of fluid flowing into tank, ℃
$T_{\mathrm{out,hx}}$	-The temperature of fluid flowing out of the heat exchanger, ℃
T_{PV}	-The temperature of photovoltaic panel, ℃
T_{ref}	-The reference temperature under STC, ℃
T_{s}	-The temperature of phase-change material in the actual
T_{tank}	-The mean temperature of tank, ℃
T_{sky}	-Sky temperature, ℃
T^*	-The absolute temperature of silica gel, K
U_{bottom}	-The heat loss coefficient at the bottom of tank
U_{edges}	-The heat loss coefficient at the edges of tank
U_{top}	-The heat loss coefficient at the top of tank
V	-Air flow velocity, m/s
v_{y}	-The vertical velocity of phase-change material under the action of gravity, m/s
W	-Moisture content of the silica gel, kg/kg
W_{fresh}	-The dehumidification capacity of supply air, g/s
Y	-The humidity ratio of wet air
Y_{w}	-The humidity ratio of isothermal wet air containing desiccant material
P_{a}	-Air density, kg/m^3
p_{s}	-The density of phase-change material, kg/m^3
φ_{w}	-The relative humidity of silica gel, %
(-)	-The angular velocity of wheel, rad/s
*(-)*in,fresh	-The moisture content of supply air at the inlet of rotary dehumidifier, g/kg
*(-)*out,fresh	-The moisture content of supply air at the outlet of rotary dehumidifier, g/kg
a	-Convective heat transfer coefficient between air and adsorbent
σ	-Stephen Boltzmann constant, W/m^2 ℃4
λ_{s}	-The thermal conductivity of phase-change material, W/(m •K)
η_{nominal}	-The photovoltaic efficiency under STC, %
η_{PV}	-Photovoltaic efficiency, %
η_{t}	-The thermal efficiency of PV/T collector, %
ε	-The surface radiation coefficient of photovoltaic panel
(τc_{n})	-The effective projected absorption product of direct light under normal incidence
IAM	-The correction coefficient of incident angle
X_{celltemp}	-The function of silicon cell efficiency and cell temperature
$X_{\mathrm{radiation}}$	-The function of silicon cell efficiency and incident radiation
Eff_{hx}	-The heat transfer efficiency of immersed heat exchanger
Eff_{T}	-Silicon cell efficiency under the reference temperature
Eff_{G}	-Silicon cell efficiency under reference spectral irradiance